PAPER

Quantum state-resolved CH$_4$ dissociation on Pt(111): coverage dependent barrier heights from experiment and density functional theory

Hirokazu Ueta,[a] Li Chen,[a] Rainer D. Beck,*[a] Inara Colón-Dìaz[b] and Bret Jackson[b]

The dissociative chemisorption of CH$_4$ on Pt(111) was studied using quantum state-resolved methods at a surface temperature (T_s) of 150 K where the nascent reaction products CH$_3$(ads) and H(ads) are stable and accumulate on the surface. Most previous experimental studies of methane chemisorption on transition metal surfaces report only the initial sticking coefficients S_0 on a clean surface. Reflection absorption infrared spectroscopy (RAIRS), used here for state resolved reactivity measurements, enables us to monitor the CH$_3$(ads) uptake during molecular beam deposition as a function of incident translational energy (E_t) and vibrational state (ν_3 anti-symmetric C–H stretch of CH$_4$) to obtain the initial sticking probability S_0, the coverage dependence of the sticking probability $S(\theta)$ and the CH$_3$(ads) saturation coverage θ_{sat}. We observe that both S_0 and θ_{sat} increase with increasing E_t as well as upon ν_3 excitation of the incident CH$_4$ which indicates a coverage dependent dissociation barrier height for the dissociation of CH$_4$ on Pt(111) at low surface temperature. This interpretation is supported by density functional calculations of barrier heights for dissociation, using large supercells containing one or more H and/or methyl adsorbates. We find a significant increase in the activation energies with coverage. These energies are used to construct simple models that reasonably reproduce the uptake data and the observed saturation coverages.

Introduction

The cleavage of a C–H bond in methane on a catalyst surface is the rate-limiting step in the transformation of natural gas into a mixture of hydrogen and carbon monoxide known as synthesis gas, which serves as the starting material for the synthesis of many bulk chemicals. Therefore, a detailed understanding of methane dissociation on the catalysts' surface is of important practical interest. In order to explore the microscopic details of the process, well-defined conditions are required. The dynamics of methane dissociation on metal surfaces has been extensively studied using molecular beams and single crystal surfaces under ultra-high vacuum conditions.[1,2] On Ni(111), the nascent reaction products CH$_3$(ads) and H(ads) are stable for $T_s < 150$ K, where CH$_3$(ads) was detected by electron energy loss spectroscopy (EELS).[3] On Pt(111), CH$_3$(ads) is stable below $T_s \sim 240$ K and was detected by reflection absorption infrared spectroscopy (RAIRS)[4] at $T_s = 150$ K as well as by high resolution X-ray photoelectron spectroscopy.[5] At a surface temperature of $T_s \sim 240$ K, CH$_3$(ads) on Pt(111) surface dehydrogenates into CH in parallel with the formation of CH$_4$(g) by recombinative

desorption of CH$_3$(ads) with H(ads).[5] For $T_s > 450$ K, CH dehydrogenation occurs leaving a carbonaceous layer on the Pt(111) surface.[6]

Previous experiments[7,8] have demonstrated that methane dissociation on transition metals is activated by both translational and vibrational energy of the incident reactant. Furthermore, quantum state-resolved studies using molecular beam techniques with state-selective infrared laser pumping showed that the methane dissociation can be both mode-specific[9] and bond-selective.[10,11] In addition to the initial conditions of the gas-phase methane reactant, the importance of the surface conditions in the reaction has also been explored. Experimental studies observe an enhancement of methane reactivity with increasing surface temperature on several transition metal surfaces.[12–16] Density functional theory (DFT)-based electronic structure calculations have revealed the role of surface lattice motion (phonons) in the reaction.[17–22] It was found that thermal displacement of the surface atoms strongly modifies the dissociation barrier height, and dissociation over surface atoms that protrude from the plane of the surface requires lower energy. Dynamical calculations showed that this leads to a strong increase in dissociative sticking with temperature.[19,20,23–26] Dissociation barrier heights also depend strongly on the surface structure. The study of CH$_4$ dissociation on Pt(533) showed an enhancement of reactivity by the step sites.[27] On the anisotropically

[a] *Laboratoire de Chimie Physique Moléculaire, Ecole Polytechnique Fédérale de Lausanne, Switzerland. E-mail: rainer.beck@epfl.ch*

[b] *Department of Chemistry, University of Massachusetts, Amherst MA 01003, USA*

20526 | *Phys. Chem. Chem. Phys.*, 2013, **15**, 20526–20535

This journal is © the Owner Societies 2013

corrugated surface, Pt(110)-(1 × 2), it was observed that the reactivity is dominated by dissociation over the ridge atoms,[28] which is consistent with both DFT[22,29,30] and dynamics[30] calculations.

Most state resolved studies of methane dissociation on transition metals published so far[31,32] report the initial sticking probability S_0 for methane incident on a bare metal surface, free of chemisorption products representing a well defined system suited for comparison with theory. The paucity of experimental information on the coverage dependent sticking probability $S(\theta)$ for methane is also due to the fact that most surface analysis methods used in previous studies cannot be applied online and *in situ* during the methane deposition as they would interfere with the methane dissociation reaction (Auger electron spectroscopy) or destroy the $CH_3(ads)$ reaction products (oxygen titration of surface carbon by temperature programmed reaction). On the theory side, the use of DFT to examine how coverage affects barrier heights requires the use of larger supercells than for the typical zero-coverage calculation. This, coupled with the already sizable problem of locating transition states for polyatomic systems makes this a computer intensive problem.

However, in real world applications of heterogeneous catalysis, the catalyst surface may be partially covered with chemisorption products, potentially changing the reaction probability and pathway. The coverage dependence of the sticking probability of CH_4 on Pt(111) has not yet been investigated in much detail either experimentally or theoretically. Here we describe a quantum state-resolved study of the dissociative chemisorption of CH_4 on Pt(111) at a surface temperature of 150 K, where the nascent dissociation products are stable and accumulate on the target surface throughout a deposition experiment. The non-invasive nature of RAIRS enables us to observe the uptake of surface-bound $CH_3(ads)$ products in real time during exposure of the Pt(111) surface to a molecular beam of state selectively prepared CH_4, yielding quantitative data on the coverage dependent state-resolved sticking probability of CH_4 on Pt(111). We find that both the initial sticking probability and the methyl saturation coverage increase with increasing translational energy and upon vibrational excitation of the incident CH_4. Our results indicate that the surface coverage of dissociation products changes the dissociation barrier height. This conclusion is supported by DFT calculations of the adsorption energies and barrier heights for methane dissociation at different product coverages. A model is constructed based on these DFT studies that reasonably reproduces the experimental uptake curve including the saturation coverages, without recourse to the usual site-blocking models, where a blocking parameter is fit to reproduce the experimental data for a particular collision energy, vibrational state, and surface temperature. This model also allows us to analyse the uptake data in a new way, extracting data on how dissociation barriers increase with increasing coverage.

Experiment

The experiments were performed in a molecular beam/surface science apparatus, the details of which have been previously published.[11,33] Briefly, the apparatus consists of a triply differentially

pumped continuous molecular beam source connected to an ultra-high vacuum chamber with a base pressure of 3 × 10^{-11} mbar. The UHV chamber contains an Ar^+ sputter gun, a residual gas analyser (RGA) and a cylindrical mirror analyser for Auger electron spectroscopy (AES). The Pt sample was mounted on a home-built manipulator and could be heated to >1300 K and cooled to 78 K.

The translational energy (E_t) of methane in the molecular beam was controlled by seeding 1–3% CH_4 in He and by variation of the nozzle temperature in the range of T_n = 300–850 K. We determined the velocity distribution of the molecular beam by time-of-flight measurements using a 200 Hz chopper wheel together with an on-axis quadrupole mass spectrometer (QMS). The measured TOF distributions are fitted to a flux weighted Maxwell Boltzman velocity distribution

$$f(v) \propto v^3 \exp\left[-\frac{m}{2kT_{\parallel}}(v - v_0)\right] \tag{1}$$

containing the stream velocity v_0 and the translation temperature $T_{\parallel}$ characterizing the width of the velocity distribution. We use $E_t = \frac{1}{2}mv_0^2$ to calculated the average incident translation energy E_t of the methane reactants. Typical widths (FWHM) of the translational energy distribution are 10–30% of E_t for nozzle temperatures of 300–850 K for the 1 and 3% CH_4 in He expansions used here.

In order to preserve the nascent methane dissociation products, $CH_3(ads)$ and H(ads), and prevent recombinative desorption,[4,34] a surface temperature of 150 K was used in all deposition experiments. The molecular beam flux of CH_4 was monitored *via* the methane partial pressure rise in the UHV chamber using a quadrupole mass spectrometer (QMS) and calibrated using a cold cathode ion gauge. The pumping speed of the system for CH_4 was determined by measuring the pump out time of the chamber using the QMS. The molecular beam spot size on the sample surface was determined by measuring carbon profiles using AES. To probe the effect of vibrational excitation, surface incident CH_4 could be prepared in a specific ro-vibrational eigenstate by infrared pumping in the molecular beam with radiation from a single-mode continuous wave optical parametric oscillator (OPO). We prepared CH_4 in the ν_3 normal mode (antisymmetric C–H stretch) *via* the R(1) ro-vibrational transition at 3038.49 cm^{-1}. The OPO frequency was stabilized to 1.5 MHz by locking to a Doppler-free Lamb dip detected in an absorption cell filled with about 30 μbar of the CH_4.[35] Excitation by rapid adiabatic passage[36] of the molecular beam through the focused IR laser beam inverts the population of the two level system formed by the $J = 1$, $\nu_3 = 0$ initial state and the $J = 2$, $\nu_3 = 1$ final state leaving approximately 50% of the incident CH_4 in the $\nu_3 = 1$, $J = 2$ eigenstate. To detect the methane dissociation products on the Pt(111) surface, an evacuated Fourier transform infrared spectrometer (FTIR, Bruker Vertex V70) was used in a reflection absorption infrared spectroscopy (RAIRS) configuration. IR radiation from the thermal source of the FTIR is reflected by the Pt(111) single crystal at near grazing incidence ($\sim 80°$) and detected using a liquid N_2 cooled InSb detector. During the exposure of the cold Pt(111)

This journal is © the Owner Societies 2013

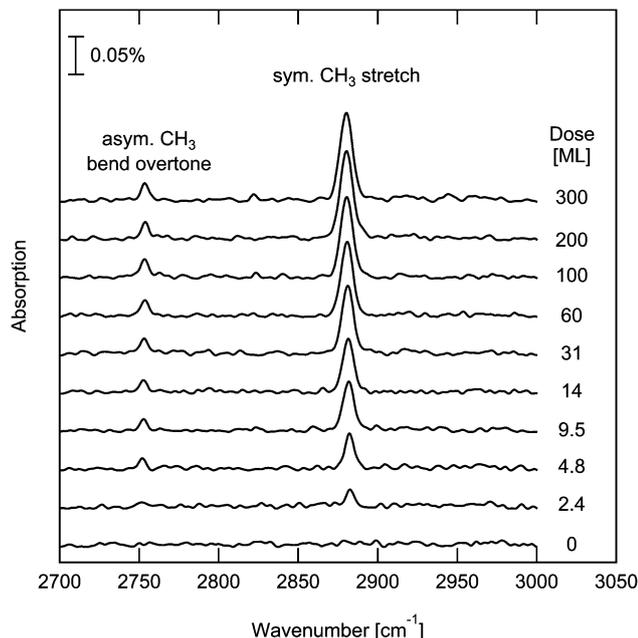*Phys. Chem. Chem. Phys.*, 2013, **15**, 20526–20535 | **20527**

Fig. 1 A series of RAIR spectra collected during molecular beam deposition of CH_4 on a Pt(111) surface at T_s = 150 K as a function of the incident CH_4 dose in monolayers (1 ML = 1.5×10^{15} molecules per cm^2). The surface bound dissociation product CH_3(ads) is detected via the CH_3 stretch absorption at 2883 cm^{-1} which, after calibration, is used to record the uptake curves shown in Fig. 2.

surface to the incident methane in the molecular beam, RAIR spectra were recorded continuously and the absorption peak intensity of the symmetric CH_3(ads) stretch at 2883 cm^{-1} was monitored as function of deposition time. The RAIR spectra presented here were recorded at a resolution of 4 cm^{-1}, averaging typically 256 sample scans in 35 seconds. Fig. 1 shows a series of RAIR spectra collected during a 40 min deposition of a CH_4 beam onto the Pt(111) surface with an average incident translational energy of E_t = 76.6 kJ mol^{-1}. Two absorption peaks emerge with increasing dose at 2883 cm^{-1} and 2755 cm^{-1} corresponding to the symmetric CH_3 stretch and a C–H bend overtone, respectively, in agreement with previous RAIRS studies.[4,34,37] We calibrate the RAIRS absorption peak intensity at 2883 cm^{-1} in terms of surface CH_3 coverage using AES detection of the carbon atoms in CH_3(ads).[33] AES detection was also used to verify that the CH_3(ads) RAIRS signal was linearly proportional to surface CH_3 coverage, for $\theta(CH_3) \leq 0.2$ ML.[33] A Pt(111) single crystal, oriented within $0.1°$ of the (111) plane, was obtained from Surface Preparation Labs. The Pt(111) surface was cleaned by repeated cycles of Ar^+ sputtering and oxygen exposure at 700 K to 5×10^{-8} mbar O_2 for 5 min, followed by annealing to 1200 K for 2 minutes. The surface cleanliness was checked by AES and could also be verified by observing the uptake of traces of CO first on the step-edge followed by the terrace sites in the RAIRS spectra.

Theory

We use the Climbing Image-Nudged Elastic Band method[38,39] to locate transition states (TS) and minimum energy paths for methane dissociation on Pt(111). Total energies are computed

using the Vienna ab initio simulation package (VASP), developed at the Institut für Materialphysik of the Universität Wien.[40–44] This code uses a plane wave basis set, and the interactions between the ionic cores and the electrons are described by fully nonlocal optimized projector augmented-wave potentials.[45] Exchange–correlation effects are treated within DFT using the Perdew–Burke–Ernzerhof (PBE) functional.[46,47] This is the functional typically used in studies of methane dissociation on metals, and the one used in our earlier bare-surface studies on Pt(111).[21,22] A supercell with periodic boundary conditions is used to model the system as a series of infinite slabs, each 4 layers thick and separated by a large vacuum spacing of 16.1 Å. To determine how surface coverage modifies the barriers to dissociation, we consider supercells containing 2×2, 3×3, and 4×4 surface unit cells, and from 0 to 8 pre-adsorbed H atoms and/or methyl groups, CH_3, in addition to the dissociating CH_4 molecule. Our approach is to initially relax the top three Pt layers and any pre-adsorbed H or CH_3, and then keep both the lattice atoms and the pre-adsorbed species fixed while locating the minimum energy path and TS for the dissociating CH_4. This is a sudden approximation: we are assuming that the reaction is fast on the timescales for lattice motion and adsorbate reorientation. While the chemisorption of methane can lead to significant lattice relaxation, our studies have shown that it is reasonable to treat the heavy lattice atoms as fixed during the short timescales of the reactive collision.[25,26] The effects of lattice motion can then be introduced into calculations of the sticking probability by thermally averaging over barrier changes due to lattice displacement.[25,26] With regard to the pre-adsorbed species, it is likely that they will not move significantly as the impinging methane approaches the surface and passes through the TS. As the H and CH_3 fragments move apart and chemisorb, there will certainly be some lattice relaxation and adsorbate rearrangement, but we are only interested here in the barrier height for the initial dissociation.

Results and discussion

a. Experiment

Having established the proportionality of the CH_3(ads) RAIRS absorption signal at 2883 cm^{-1} and the CH_3(ads) coverage by comparison with AES detection,[9] we use RAIRS to record CH_3(ads) uptake curves which relate the product coverage $\theta(CH_3)$ to the incident dose $D(CH_4)$ of methane. Fig. 2(a) shows several RAIRS detected uptake curves for incident translational energies E_t in the range of 46.3–76.6 kJ mol^{-1} without laser excitation. The coverage dependent sticking coefficient $S(\theta)$ is obtained as the derivative of the uptake curve with respect to the dose D:

$$S(\theta) = d\theta(CH_3)/dD(CH_4) \qquad (2)$$

which can be seen to decrease in Fig. 2 with increasing $\theta(CH_3)$. To extract $S(\theta)$ from the data, we fit a Langmuir uptake model for dissociative adsorption[16] to the RAIRS uptake data resulting in the solid lines shown in Fig. 2.

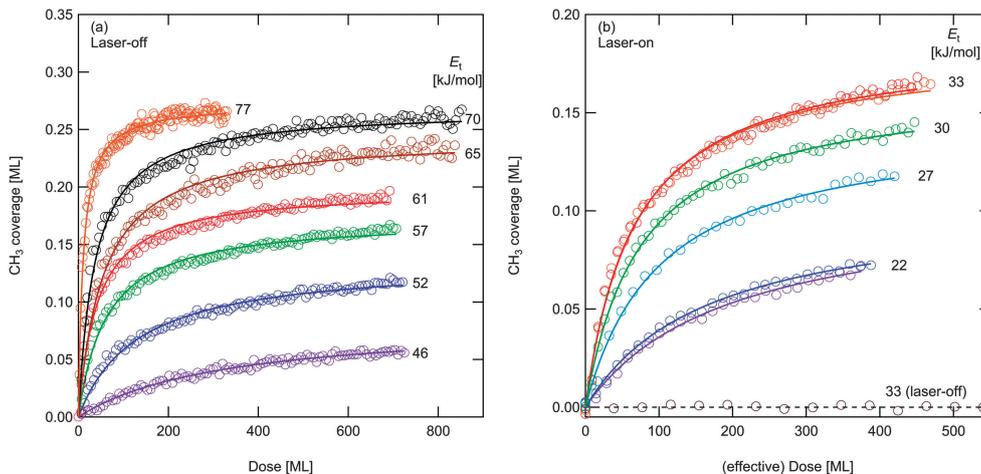$$\theta(CH_3) = \theta_{sat}\frac{B \cdot D}{1 + B \cdot D} \qquad (3)$$

Fig. 2 (a) RAIRS detected CH_3(ads) uptake curves relating methyl coverage to the incident CH_4 dose for different incident translational energies E_t in the range of 46–77 kJ mol^{-1} for laser-off conditions. (b) Laser-on (ν_3-excitation) uptake curves for incident ν_3-excited $CH_4(\nu_3)$ for E_t in the range of 22–33 kJ mol^{-1}. Effective dose refers to the incident dose of $CH_4(\nu_3)$ only. For comparison, the laser-off (E_t = 33 kJ mol^{-1}) result is also shown to demonstrate that the observed methyl coverage is only due to incident $CH_4(\nu_3)$. Note that for $CH_4(\nu_3)$, a given saturation coverage is achieved at much lower E_t compared to the laser-off depositions.

where the fitting parameters are the constant B and the CH_3 saturation coverage θ_{sat}, and D is the measured molecular beam dose. The model assumes that CH_4 dissociation requires two adjacent surface vacancies for CH_3(ads) and H(ads) leading to faster than linear decrease of the reactivity with coverage. The initial sticking probability S_0 on the clean surface (θ = 0) is calculated as the initial slope of the uptake curve from the product of the fitting parameters θ_{sat} and B:

$$S_0 = \theta_{sat} \cdot B \qquad (4)$$

Fig. 3(a) shows the initial sticking probabilities S_0 as function of E_t for the laser-off and laser-on depositions. For the three highest values of S_0 in the laser-off dataset, the uptake was too fast to determine an accurate value of S_0 from the RAIRS data due to the fact that a significant coverage was deposited

during the initial 30 s RAIRS data collection interval. Therefore the value of S_0 was measured by the King and Wells method[48] (0.5 s averaging) performed simultaneously with the RAIRS detection for each deposition. The laser-off data represents an averaged reactivity over the thermally excited vibrational levels populated at the nozzle temperature of each experiment. Based on data reported by Luntz and Bethune who studied the change in S_0 between T_n = 300 K and 680 K over same E_t range,[12] we estimate the true ground state reactivity $S_0(\nu = 0)$ to be lower by a factor of 2 than our S_0(laser-off) measured at T_n = 680 K.

The results show that both the initial sticking probability S_0 *and* the saturation coverage $\theta_{sat}(CH_3)$ depend on the translational energy E_t of the incident CH_4. This is in contrast to previous CH_4 reactivity measurements on Pt(111) and Ni(111) performed at higher surface temperatures (T_s > 400 K) where
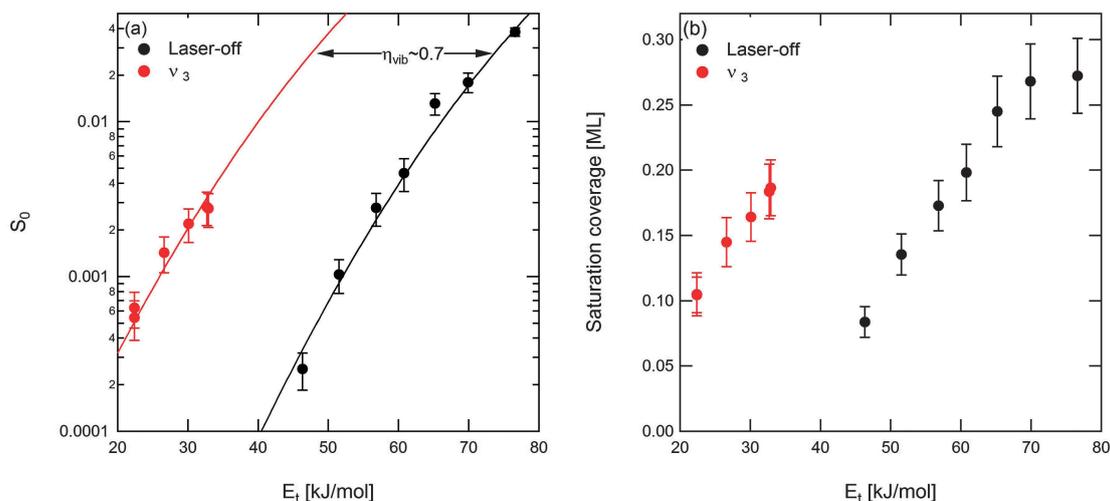

Fig. 3 (a – left) Initial sticking probability S_0 for CH_4 on Pt(111) as function of E_t without laser excitation (black – laser-off) and with state specific excitation of the ν_3 mode (red). The solid lines are S-shaped reactivity curves fitted to the data to extract a vibrational efficacy of $\eta(\nu_3)$ = 0.7. (b – right) CH_3(ads) saturation coverage as a function of translational energy E_t for laser-off (black) and ν_3 excitation (red).

the nascent methyl products quickly dehydrogenate and the adsorbed hydrogen leaves the surface by recombinative desorption, leaving only carbon atoms on the surface.[49] Under such conditions the saturation coverage of carbon was found to be independent of the incident translational energy or vibrational excitation.[1] Fig. 2(b) shows the laser-on uptake curves for $CH_4(\nu_3)$, prepared via IR laser pumping with one quantum of ν_3 vibration (antisymmetric C–H stretch) for several values of E_t. Compared to the laser-off experiments, E_t was reduced by lowering T_n within the range $T_n = 294$ to 408 K for the 3% CH_4 in He beam. For comparison, a 60 min laser-off deposition of the 3% CH_4 in He beam with $T_n = 408$ K ($E_t = 32.8$ kJ mol^{-1}) produces no detectable CH_3(ads) coverage indicating that the laser-off reactivity of CH_4 is negligible in all of the laser-on depositions. Therefore the laser-on experiments directly reflect the state-resolved reactivity of $CH_4(\nu_3 = 1, J = 2)$. The laser-on RAIRS data of Fig. 2(b) is again fitted by our Langmuir uptake model to extract the state-resolved initial sticking probability $S_0(\nu_3)$ and the saturation coverage $\theta_{sat}(\nu_3)$ presented Fig. 3. For quantitative comparison of the effect of translation and ν_3 excitation, we fit the laser-off and laser-on results with the S-shaped reactivity curves proposed by Luntz,[50]

$$S_0 = \frac{A}{2}\left[1 + \text{erf}\left(\frac{E_t - E_0}{W}\right)\right] \qquad (5)$$

where A is the asymptotic value of S_0 for $E_t \rightarrow \infty$ taken to be unity here, E_0 the average barrier height and W is the width of the distribution of barrier heights assumed to be Gaussian. Laser-off and laser-on reactivity data were fitted with $A = 1$ and a width parameter $W = 26$ kJ mol^{-1} to determine the average barrier height E_0(laser-off) and $E_0(\nu_3)$ for the two datasets. The vibrational efficacy $\eta(\nu_3)$ is determined by the horizontal offset between the two fitted S-curves, $\Delta E_0(\nu_3) = E_0(\text{laser-off}) - E_0(\nu_3)$, and the vibrational energy of the state, $h\nu_3$:

$$\eta(\nu_3) = \frac{\Delta E_0(\nu_3)}{h\nu_3} = 0.71 \qquad (6)$$

For comparison, we have previously determined the vibrational efficacy for $2\nu_3$ overtone excitation, finding that $\eta(2\nu_3) = 0.38$ for CH_4 dissociation on Pt(111) at $T_s = 600$ K.[49] Both the vibrational efficacies $\eta(\nu_3)$ and $\eta(2\nu_3)$ are observed to be lower for Pt(111) than on Ni(111) ($\eta(\nu_3) = 1.25$,[51] $\eta(2\nu_3) = 0.65$ (ref. 13)). This suggests that there is a smaller extension of the dissociating C–H bond at the transition state, indicating an "earlier barrier" for Pt(111) than for Ni(111), which is consistent with recent DFT calculations.[21] We turn our attention to the observed changes in CH_3 saturation coverage, θ_{sat}. Fig. 3(b) shows how θ_{sat} depends on the CH_4 translational energy for both laser-off and laser-on depositions. In both cases θ_{sat} increases with increasing E_t and for the laser-off depositions approaches an asymptotic value near 0.25 ML at high E_t. To confirm that the change in θ_{sat} coverage is due to the variation of E_t and to exclude the possibility of site blocking effects by the adsorption of potential contaminants in the molecular beam such as H_2, H_2O, and CO, we performed the following test. First the Pt(111) surface was exposed to a molecular beam of CH_4 with $E_t = 44.5$ kJ mol^{-1} (laser-off conditions) while the CH_3 uptake was followed by RAIRS. When the uptake
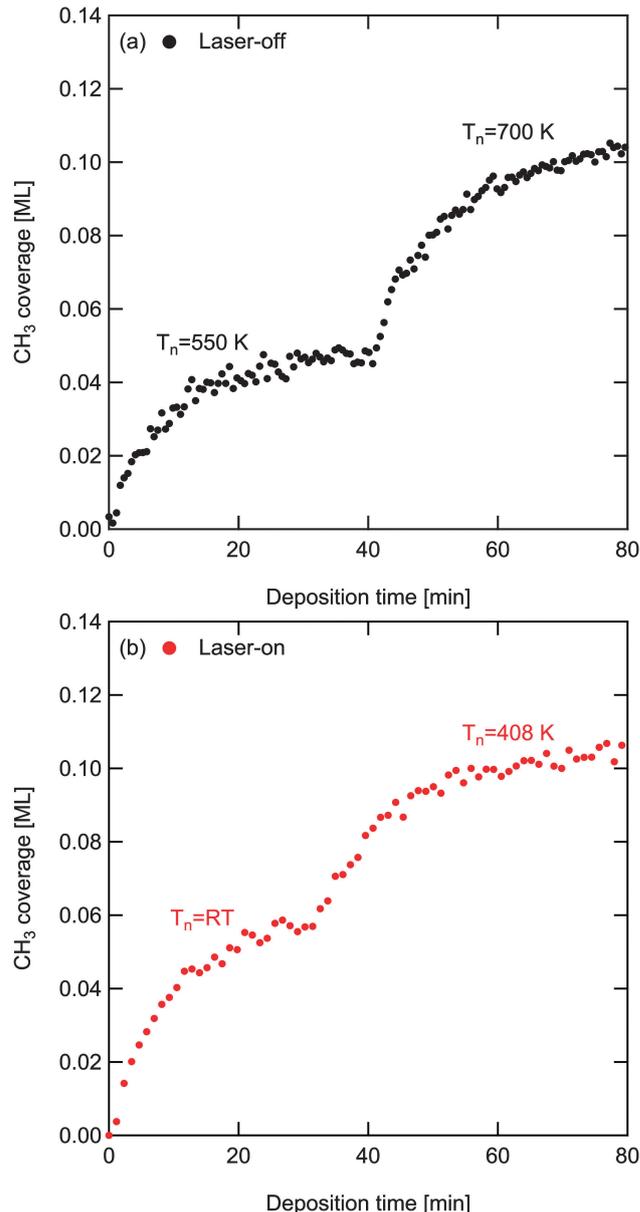

Fig. 4 (a) CH_3 uptake for $CH_4(\nu = 0)$ (laser-off) and (b) $CH_4(\nu_3)$ (laser-on) exposure of Pt(111) at $T_s = 150$ K. Once the uptake curve approaches a first saturation level (after ∼40 min of deposition), E_t was increased as indicated in the figure resulting in (1) increased reactivity as demonstrated by the change in slope of the uptake curve and (2) an increase in the saturation coverage as indicated by the higher asymptote. This shows that the level of the saturation coverage is controlled only by the reactivity of the incident methane and not due to site block effects of any other species not detected by RAIRS.

approached a saturation coverage of 0.05 ML, the incident translational energy of CH_4 was increased to $E_t = 57.4$ kJ mol^{-1}. With increased E_t, we detect a renewed uptake on the same surface, approaching a higher saturation coverage of 0.12 ML shown in Fig. 4(a). Similarly, Fig. 4(b) shows that for a laser-on $CH_4(\nu_3)$ deposition with $E_t = 22.5$ kJ mol^{-1} the coverage approaches saturation but then continues to grow once E_t is increased to 32.2 kJ mol^{-1}. A variation in CH_3(ads) saturation coverage on Pt(111) with E_t has previously been reported by

20530 | Phys. Chem. Chem. Phys., 2013, **15**, 20526–20535
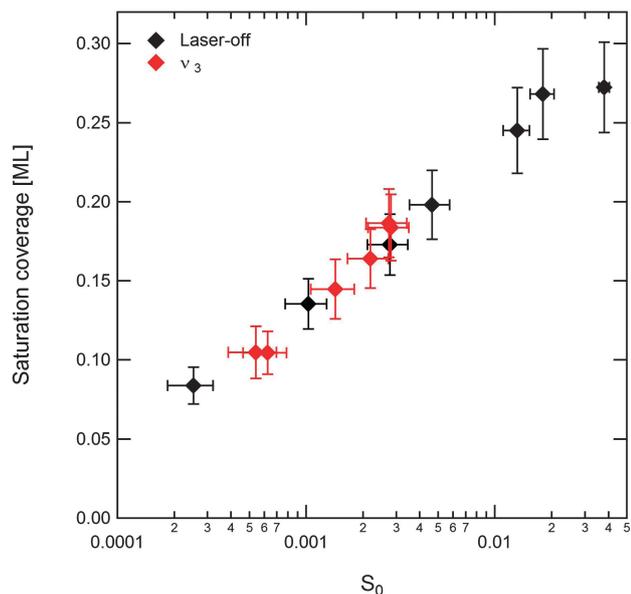
This journal is © the Owner Societies 2013

Fig. 5 $CH_3(ads)$ saturation coverage as a function of initial CH_4 sticking probability S_0(laser-off) and $S_0(\nu_3)$. Both the laser-off and the ν_3-data fall on a common curve relating the saturation coverage to the reaction probability of the incident methane. This suggests that the saturation coverage is simply a function of CH_4 reactivity, irrespective if the dissociation is activated by translational energy E_t or by ν_3-excitation, consistent with a coverage dependent reaction barrier height.

Fuhrmann et al.[6] who used high-resolution X-ray photoelectron spectroscopy to monitor the CH_3 uptake on Pt(111) at T_s = 120 K for E_t in the range of 30–80 kJ mol^{-1}. Fuhrmann et al. speculated that an increase in impact energy might lead to the displacement of adsorbed hydrogen, H(ads), freeing additional sites where CH_3 can adsorb.

In our study presented here, we observe an increase in θ_{sat} not only upon increasing E_t but also upon vibrational excitation of the ν_3 mode. Comparing the data of Fig. 3(a) and (b), we find that deposition of $CH_4(\nu_3)$ results in similar reactivity and saturation coverage at an incident E_t which is lower by ~ 26 kJ mol^{-1} than what is observed in the deposition without laser excitation of ν_3. In fact, if we plot θ_{sat} as a function of S_0 (Fig. 5), the laser-off and laser-on data overlap on a common curve, consistent with the idea that θ_{sat} is controlled by the CH_4 reactivity, which in turn is determined both by incident translational energy and the vibrational state. This leads us to propose that the observed changes in saturation coverage are due to a variation of the CH_4 dissociation barrier height with product coverage.

b. DFT calculations

The barrier height for the dissociative adsorption on different transition metal surfaces is connected to the adsorption energy via the well known Brønsted–Evans–Polanyi (BEP) relationship.[52,53] On a given metal surface, the adsorption energy tends to decrease with increasing adsorbate coverage due to interactions between the adsorbates or adsorbate induced changes in the electronic structure of the metal. Therefore a decrease in adsorption energy with increasing product coverage will cause an increase in barrier height consistent with the observed changes in $CH_3(ads)$

saturation coverage. This is precisely the behaviour we observe in our DFT studies.

Earlier DFT studies of methane dissociation on Pt(111), using a 2×2 supercell with no pre-adsorbed H or CH_3, identified 6 transition states.[21,22] In all cases the carbon atom is over the top site at the TS and remains there after the reaction, as the methyl group preferentially binds to the top site by 0.6–0.9 eV relative to other sites. The adsorption energy of H is largest at the fcc hollows, but only by 50 meV relative to the top, bridge and hcp sites.[21] As a consequence, the adsorbed H atoms are mobile at the temperatures of the experiment, and the barriers to dissociation do not vary dramatically with the orientation of the dissociating H. The lowest activation energy, the height of the TS barrier relative to the methane far above the surface, is $E_a = 0.93$ eV, corresponding to the dissociating H moving along the bridge towards a neighboring top site. Dissociation paths with the H moving towards the fcc or hcp hollows are only slightly less favored, with $E_a = 0.95$ to 0.98 eV, depending upon the orientation of the methyl group. Zero point energy corrections lower all of these barriers by about 0.11 eV.[21,22] As this correction is roughly the same for all of the barriers computed here, we will not include it in the reported values for E_a.

The energetics for recombinative desorption in these experiments are not favourable. The adsorbed methyl groups are not mobile at 150 K, and the barrier to formation of methane is large. The adsorbed H are mobile, but using the DFT values computed at $\frac{1}{4}$ ML (the 2×2 supercell) we find that formation of $H_2(g)$ from 2 equilibrated adsorbed H atoms is uphill by 0.71 eV, including zero point energies. The dissociative adsorption of methane is only weakly exothermic, by 0.02 eV, for H and CH_3 at infinite separation. Thus, the laser off threshold for H_2 recombination via a hot atom process is $E_t = 0.7$ eV, ignoring any energy loss to phonons or other degrees of freedom, and this type of process is not likely to be the source of an energy-dependent saturation coverage.

We have computed E_a for several different coverages. In all cases the dissociating H is oriented along a bridge site. What we call the product state is the last image in the NEB calculation, corresponding to the dissociated H on the neighbouring top site. Figures showing the geometry of these transition and product states, along with tables of corresponding geometric and energetic data, can be found in ref. 21 and 22, where this particular reaction path is denoted as D2. For the 2×2 supercell, $E_a = 0.93$ eV and the product energy $E_p = 0.31$ eV. As we decrease the coverage from $\frac{1}{4}$ ML to 1/9 ML and 1/16 ML by using 3×3 and 4×4 supercells, E_p drops to 0.23 and 0.19 eV, and as expected, E_a drops to 0.89 and 0.86 eV, respectively. Extrapolating, we estimate that the barrier is about 0.84 eV in the limit of zero coverage. While this certainly suggests an increase in E_a with coverage, the situation is artificial in the sense that the methane and all of its repeated images are dissociating at the same time. We thus consider the case of dissociation in the presence of pre-adsorbed H and CH_3, using our large 4×4 supercell to minimize the repulsion between the dissociating methane and its repeated images.

This journal is © the Owner Societies 2013

Phys. Chem. Chem. Phys., 2013, **15**, 20526–20535 | **20531**

To simulate an initial coverage of 1/16 ML, we pre-adsorb one methyl at a top site, and one H at an fcc site two hollows away, in one quadrant of our 4×4 cell. There are three sites in the cell where dissociative adsorption of a second CH_4 is most energetically feasible, corresponding to the three "empty" quadrants of our 4×4 cell, and these have product energies $E_p = 0.23, 0.38$ and 0.46 eV. For dissociation at these three sites, we find $E_a = 0.90, 0.94$ and 1.04 eV, respectively. If we pre-adsorb two methyl groups and two H atoms, in two adjacent quadrants of our cell, we similarly find two remaining sites with relatively low barriers to dissociation left open. These have product energies $E_p = 0.34$ and 0.69 eV, and corresponding dissociation barriers $E_a = 0.92$ and 0.99 eV. Pre-adsorbing 3 methyls and 3 H leaves only one site in the 4×4 cell open, with $E_p = 0.47$ eV and $E_a = 0.92$ eV. Thus, we observe a significant increase in E_a with coverage, and these are minimum values, as we have only considered the lowest energy pathways available.

All of the above configurations correspond to situations where the carbon atoms are at least two lattice spacings apart, and no H atoms reside in any of the hollow sites adjacent to the carbons. Going beyond this leads to even larger increases in E_p, and correspondingly, E_a. We have considered three such situations. In the first, we dissociate methane over a top site, in a 3×3 supercell, with a pre-adsorbed H atom in the adjoining fcc hollow. There are three fcc sites in which to put this H, and we choose the lowest energy configuration where the H is on the fcc hollow furthest away from the dissociating C–H bond. We find that E_p increases to 0.45 eV, while the barrier increases by 0.2 eV to 1.10 eV. We also consider the dissociation of methane, again in a 3×3 supercell, with a pre-adsorbed CH_3 group in a neighbouring top site. We again take the lowest energy case where the pre-adsorbed methyl is furthest away from the dissociating H. We find $E_p = 0.61$ eV and $E_a = 1.14$ eV, corresponding to an increase in the barrier height of 0.24 eV. Finally, we find these effects to be roughly additive, and it is very unfavourable, energetically, to go beyond a coverage of $\frac{1}{4}$ ML. This coverage corresponds to one methyl on every other Pt atom in a 2×2 array, with the H atoms in fcc hollows in a staggered 2×2 array. We have attempted to insert a fifth H and CH_3 into a 4×4 supercell already containing 4 methyls and 4 H atoms, and the lowest E_p we have found is about 1.73 eV, for the sudden case where the pre-adsorbed species remain fixed. The corresponding barrier is likely to be so large as to prevent dissociation at coverages above $\frac{1}{4}$ ML. This is consistent with the experimental data in Fig. 2, 3(b) and 5.

c. Adsorption model

Clearly, E_a can increase significantly as coverage increases, but how do we quantitatively relate the DFT data and the experimental θ *vs.* D uptake curves? Consider the following model for adsorption, where, given our arguments against recombinative desorption, we set $\theta(CH_3) = \theta(H) = \theta$:

$$\frac{d\theta}{dD} = \sum_j P_j(\theta) S_j(E_t, \nu) \tag{7}$$

The index j labels all of the possible environments that might exist for dissociation at a coverage θ. These include, for example, dissociation over a top site with no adsorbates in the vicinity, dissociation where there is one adsorbed CH_3 two sites away, and so on. P_j is the probability for each configuration, at a coverage θ, and S_j is the dissociative sticking probability for this configuration, which depends upon E_t and whether or not the ν_3 stretch is excited, $\nu = 1$ or 0, respectively. The $\theta = 0$ sticking data are well described by the empirical expression:

$$S_0(E_t, \nu) = be^{\alpha(E_t + c\nu)} \tag{8}$$

where $c = \eta(\nu_3) h\nu_3$ and a least squares fit to the data in Fig. 3 yields $\alpha = 0.172$ (kJ mol^{-1}).

It is reasonable to approximate

$$S_j(E_t, \nu) = be^{\alpha(E_t + c\nu - \Delta_j)} = S_0 e^{-\alpha \Delta_j} \tag{9}$$

where Δ_j is the increase in dissociation barrier height for configuration j, relative to the zero coverage case. This approximation is based on the assumption that while the barrier height may change with adsorbate coverage, the morphology of the potential energy surface in the vicinity of the TS is not otherwise modified appreciably. We have successfully used this "energy-shifting" approximation to average S over surface impact sites and lattice atom displacements.[23,24] Unfortunately, it is only feasible to compute Δ_j for a few of the hundreds of configurations likely to be important. However, we can get a rough estimate of the magnitude of Δ_j and how it varies with coverage by making the following approximation:

$$\frac{d\theta}{dD} = \sum_j P_j(\theta) S_j(E_t, \nu) \approx S_0 \sum_j P_j(\theta) e^{-\alpha \Delta_j} \approx S_0 (1 - \theta)^2 e^{-\alpha \Delta_{av}} \tag{10}$$

where $\Delta_{av}(\theta)$ is, roughly speaking, the average Δ_j at a coverage θ, and $(1 - \theta)^2$ is the probability of finding two open adjacent top sites, allowing for dissociative sticking. We use eqn (10) to extract $\Delta_{av}(\theta)$ from the experimental data by computing $d\theta/dD$ from the eqn (3) fits. Using the fit value for α and the experimental values for S_0, we get the curves in Fig. 6. As the uptake curves shown in Fig. 2 saturate, $\Delta_{av}(\theta)$ can spike to large values. However, for both the laser off and the ν_3 data there is a continuous and roughly linear increase in $\Delta_{av}(\theta)$ with θ, and both datasets give the same slope. Our DFT calculations are in good agreement with these curves. In our studies with a 4×4 supercell, we found that for initial adsorbate coverages between 1/16 and 3/16 ML the barrier increased by values in the range 0.04–0.18 eV. These values agree well with the extracted data, keeping in mind that $\Delta_{av}(\theta)$ is a rough average and that the computed DFT values correspond to the smallest of what is likely to be a broad distribution of barriers. At higher coverage, where an incident methane is more likely to collide with a Pt atom adjacent to an adsorbed H atom or CH_3, we computed (minimum) barrier increases of 0.20 and 0.24 eV, respectively, in good agreement with $\Delta_{av}(\theta)$ at higher values of θ. Again, these barriers were for adsorbate positions away from the

20532 | *Phys. Chem. Chem. Phys.,* 2013, **15**, 20526–20535
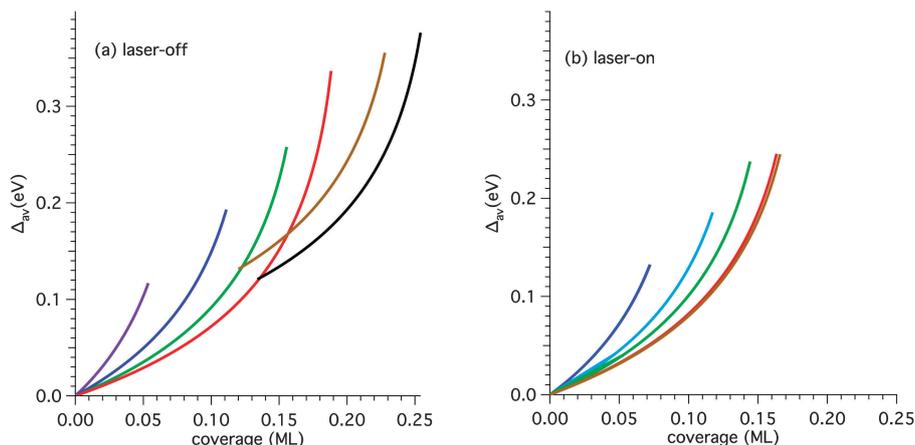
This journal is © the Owner Societies 2013

Fig. 6 Mean increase in barrier height, $\Delta_{av}(\theta)$, as a function of coverage, extracted from the data in Fig. 2, using eqn (7) in the text, for (a), the laser-off case, and (b), the laser-on case. The curves are color-coded to correspond to the curves in Fig. 2.

dissociating H, and other configurations of the molecule are likely to lead to even higher barriers.

Two questions remain: can we put together an approximate but first principles model for dissociative sticking based on the DFT data, and is such a model capable of reproducing a saturation coverage that varies with the incident energy and vibrational state of the methane? The Langmuir model of eqn (3) fits the data well, but requires that a different θ_{sat} be fit to each dataset (E_t, v). This θ_{sat} is often interpreted in terms of site blocking, and indeed, eqn (3) is a solution of

$$\frac{d\theta}{dD} = S_0(1 - \eta\theta)^2 \qquad (11)$$

where $\eta = \theta_{sat}^{-1}$ is the number of sites "blocked" by the adsorbed H and CH_3. Eqn (11) corresponds to a lattice model where two adjacent sites are required for dissociation, and each adsorbate blocks η sites. Of course, this is a semi-empirical model designed to fit curves that saturate rigorously at $\theta = \eta^{-1} < 1$. In reality, except for the top sites containing the adsorbed CH_3, no other top sites are physically blocked by the adsorbates. The actual physics is that $\eta = 1$ and the barrier

to dissociation at unblocked sites increases with increasing coverage, and there are many different environments for dissociation, all with different barrier heights, as described by eqn (7). That is, S_j is neither equal to 0 or to S_0, but something in between. While we have only examined a few of the many possible adsorbate configurations of eqn (7), we can put together the following model based on eqn (7)–(9), and our DFT results. The lowest barriers correspond to the case where there are no adsorbates on sites adjacent to the CH_4 as it dissociates. For this we need an open top site, with no methyl groups adsorbed on the adjacent 6 top sites, and no H atoms in the 3 adjacent fcc hollows. Since $\theta(H) = \theta(CH_3) = \theta$, the probability that the incident molecule finds these 10 open sites is $P_1 = (1 - \theta)^{10}$. These are the types of configurations considered in our studies using the large 4×4 supercell. We found that the barriers increased slowly with coverage, and we approximate this increase as $\Delta_1 = (0.65 \text{ eV ML}^{-1})\cdot\theta$, where the value 0.65 eV ML^{-1} is an average of our 3 lowest computed values for initial coverages of 1/16, 1/8 and 3/16 ML. We thus approximate $S_1 = S_0 \exp(-\alpha\Delta_1)$, as in eqn (9). The probability of finding the P_1 configuration, but with either one CH_3 or one H
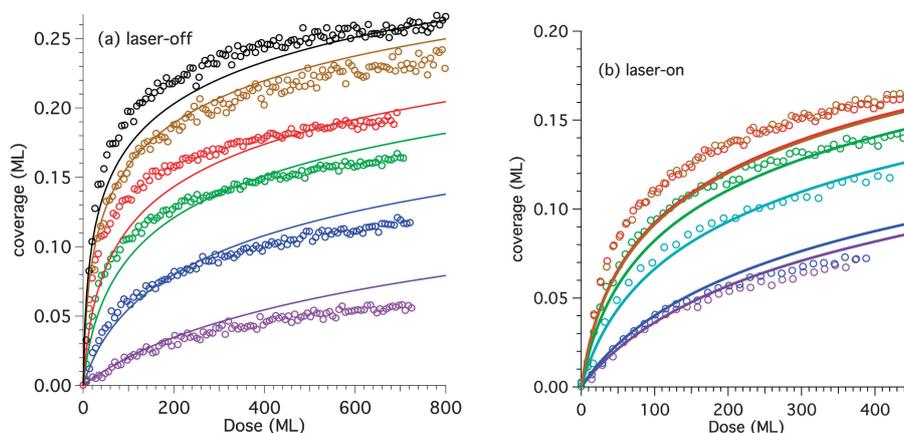

Fig. 7 Coverage as a function of dose, for (a), the laser-off case, and (b), the laser-on case. The lines correspond to the theory presented in the text, and the circles are the data from Fig. 2. The lines and circles correspond to the color-coding in Fig. 2.

This journal is © the Owner Societies 2013

Phys. Chem. Chem. Phys., 2013, **15**, 20526–20535 | **20533**

adsorbed adjacent to the impact site, is $P_2 = 8 (1 - \theta)^9 \theta$. We have shown that for these cases the barriers increase by about $\Delta = 0.22$ eV, and we write $S_2 = S_1 \exp(-\alpha\Delta)$. Similarly, the probability of finding the P_1 configuration, but with 2 adsorbates next to the impact site, is $P_3 = 28(1 - \theta)^8 \theta^2$, and we write $S_3 = S_1 \exp(-2\alpha\Delta)$. We include two more terms in this sum, P_4 and P_5, though they don't significantly modify the results, plotted in Fig. 7 along with the experimental data of Fig. 2. The agreement is remarkably good, given the simplicity of the model. We use only the DFT data, the measured $S_0(E_t, \nu)$, and the parameter α extracted from the S_0 data. More importantly, it is clear that we can get saturation effects without invoking a blocking parameter that is fit to the data for each (E_t, ν). It is likely that we could tweak the model to get a better fit, but to accurately reproduce the data would require that we remove the separability assumption of eqn (9), computing potential energy surfaces for numerous configurations j and computing S_j, an impossible task. It is perhaps surprising that this assumption works as well as it does. Note that this separability leads to a rate proportional to $S_0(E_t, \nu)f(\theta)$, where f is some function of the coverage. Given our value for α, $f(\theta)$ drops by about three orders of magnitude when the effective barriers increase by about 0.4 eV. That is, the curves effectively saturate on experimental timescales when the rate drops below some value $R_{min} = S_0 \exp(-\alpha\theta_{sat})$, and thus this first order model suggests that θ_{sat} is proportional to $\ln(S_0)$, the experimental result in Fig. 5. Given eqn (9), θ_{sat} is also therefore proportional to E_t, as illustrated in Fig. 3(b). Thus this simple DFT-based model is qualitatively consistent with all of the experimental observations.

Conclusion

We have measured the state-resolved sticking probability and saturation coverage for CH_4 dissociation on Pt(111) at a surface temperature of 150 K as a function incident translational energy and vibrational state. State specific ν_3 excitation enhances CH_4 dissociation on Pt(111) reaction with an efficacy of 0.7 compared to translational energy. We observe that the CH_3 saturation coverage, $\theta_{sat}(CH_3)$, increases with translational energy and also upon ν_3-excitation indicating that $\theta_{sat}(CH_3)$ is a function of CH_4 reactivity. This indicates that there is a product coverage dependence of the activation barrier height.

DFT studies confirm these predictions. We compute barrier heights for dissociation using large supercells containing one or more adsorbates, and find significant increases in the activation energies with increasing coverage. Our DFT results are consistent with an increase in the coverage-dependent mean barrier height that we extract from the experimental data. Moreover, simple models for the coverage as a function of dose reasonably reproduce the data and the observed saturation coverages. This saturation coverage is shown to increase with the log of S_0, which is proportional to the collision energy below saturation, in full agreement with the experimental findings.

Acknowledgements

References

1. J. H. Larsen and I. Chorkendorff, *Surf. Sci. Rep.*, 1999, **35**, 163–222.
2. J. F. Weaver, A. F. Carlsson and R. J. Madix, *Surf. Sci. Rep.*, 2003, **50**, 107–199.
3. M. B. Lee, Q. Y. Yang, S. L. Tang and S. T. Ceyer, *J. Chem. Phys.*, 1986, **85**, 1693–1694.
4. D. J. Oakes, M. R. S. McCoustra and M. A. Chesters, *Faraday Discuss.*, 1993, **96**, 325–336.
5. T. Fuhrmann, M. Kinne, C. M. Whelan, J. F. Zhu, R. Denecke and H. P. Steinrück, *Chem. Phys. Lett.*, 2004, **390**, 208–213.
6. T. Fuhrmann, M. Kinne, B. Tränkenschuh, C. Papp, J. F. Zhu, R. Denecke and H.-P. Steinrück, *New J. Phys.*, 2005, **7**, 107.
7. C. T. Rettner, H. E. Pfnür and D. J. Auerbach, *Phys. Rev. Lett.*, 1985, **54**, 2716–2719.
8. A. C. Luntz and D. S. Bethune, *J. Chem. Phys.*, 1989, **90**, 1274–1280.
9. R. D. Beck, P. Maroni, D. C. Papageorgopoulos, T. T. Dang, M. P. Schmid and T. R. Rizzo, *Science*, 2003, **302**, 98–100.
10. D. R. Killelea, V. L. Campbell, N. S. Shuman and A. L. Utz, *Science*, 2008, **319**, 790–793.
11. L. Chen, H. Ueta, R. Bisson and R. D. Beck, *Faraday Discuss.*, 2012, **157**, 285–295.
12. A. C. Luntz and D. S. Bethune, *J. Chem. Phys.*, 1989, **90**, 1274–1280.
13. P. M. Holmblad, J. Wambach and I. Chorkendorff, *J. Chem. Phys.*, 1995, **102**, 8255–8263.
14. D. C. Seets, C. T. Reeves, B. A. Ferguson, M. C. Wheeler and C. B. Mullins, *J. Chem. Phys.*, 1997, **107**, 10229–10241.
15. R. C. Egeberg, S. Ullmann, I. Alstrup, C. B. Mullins and I. Chorkendorff, *Surf. Sci.*, 2002, **497**, 183–193.
16. D. R. Killelea, V. L. Campbell, N. S. Shuman, R. R. Smith and A. L. Utz, *J. Phys. Chem. C*, 2009, **113**, 20618–20622.
17. G. Henkelman and H. Jónsson, *Phys. Rev. Lett.*, 2001, **86**, 664–667.
18. G. Henkelman, A. Arnaldsson and H. Jónsson, *J. Chem. Phys.*, 2006, **124**, 044706.
19. S. Nave and B. Jackson, *Phys. Rev. Lett.*, 2007, **98**, 173003.
20. S. Nave and B. Jackson, *J. Chem. Phys.*, 2007, **127**, 224702–224711.
21. S. Nave and B. Jackson, *J. Chem. Phys.*, 2009, **130**, 054701–054714.
22. S. Nave, A. K. Tiwari and B. Jackson, *J. Chem. Phys.*, 2010, **132**, 054705.
23. B. Jackson and S. Nave, *J. Chem. Phys.*, 2011, **135**, 114701.
24. B. Jackson and S. Nave, *J. Chem. Phys.*, 2013, **138**, 174705.
25. A. K. Tiwari, S. Nave and B. Jackson, *Phys. Rev. Lett.*, 2009, **103**, 253201.

20534 | *Phys. Chem. Chem. Phys.*, 2013, **15**, 20526–20535

This journal is © the Owner Societies 2013

26 A. K. Tiwari, S. Nave and B. Jackson, *J. Chem. Phys.*, 2010, **132**, 134702–134709.

27 A. T. Gee, B. E. Hayden, C. Mormiche, A. W. Kleyn and B. Riedmuller, *J. Chem. Phys.*, 2003, **118**, 3334–3341.

28 R. Bisson, M. Sacchi and R. D. Beck, *J. Chem. Phys.*, 2010, **132**, 094702–094709.

29 A. Anghel, D. Wales, S. Jenkins and D. King, *Phys. Rev. B: Condens. Matter Mater. Phys.*, 2005, **71**, 113410.

30 D. Han, S. Nave and B. Jackson, *J. Phys. Chem. A*, 2013, **117**, 8651–8659.

31 L. B. F. Juurlink, D. R. Killelea and A. L. Utz, *Prog. Surf. Sci.*, 2009, **84**, 69–134.

32 R. D. Beck and A. L. Utz, in *Dynamics of Gas-Surface Interactions Dynamics of Gas-Surface Interactions*, ed. R. B. Diez Muino and H. Fabio, Springer, Heidelberg, New York, 2013, vol. 50, pp. 179–212.

33 L. Chen, H. Ueta, R. Bisson and R. D. Beck, *Rev. Sci. Instrum.*, 2013, **84**, 053902–053909.

34 D. J. Oakes, H. E. Newell, F. J. M. Rutten, M. R. S. McCoustra and M. A. Chesters, *J. Vac. Sci. Technol., A*, 1996, **14**, 1439–1447.

35 B. L. Yoder, R. Bisson, P. M. Hundt and R. D. Beck, *J. Chem. Phys.*, 2011, **135**, 224703–224709.

36 N. V. Vitanov, T. Halfmann, B. W. Shore and K. Bergmann, *Annu. Rev. Phys. Chem.*, 2001, **52**, 763–809.

37 D. H. Fairbrother, X. D. Peng, M. Trenary and P. C. Stair, *J. Chem. Soc., Faraday Trans.*, 1995, **91**, 3619–3625.

38 G. Henkelman and H. Jónsson, *J. Chem. Phys.*, 2000, **113**, 9978–9985.

39 G. Henkelman, B. P. Uberuaga and H. Jónsson, *J. Chem. Phys.*, 2000, **113**, 9901–9904.

40 G. Kresse and J. Hafner, *Phys. Rev. B: Condens. Matter Mater. Phys.*, 1993, **47**, 558–561.

41 G. Kresse and J. Hafner, *Phys. Rev. B: Condens. Matter Mater. Phys.*, 1994, **49**, 14251–14269.

42 G. Kresse and J. Furthmuller, *Phys. Rev. B: Condens. Matter Mater. Phys.*, 1996, **54**, 11169–11186.

43 G. Kresse and J. Furthmuller, *Comput. Mater. Sci.*, 1996, **6**, 15–50.

44 G. Kresse and D. Joubert, *Phys. Rev. B: Condens. Matter Mater. Phys.*, 1999, **59**, 1758–1775.

45 P. E. Blöchl, *Phys. Rev. B: Condens. Matter Mater. Phys.*, 1994, **50**, 17953–17979.

46 J. P. Perdew, K. Burke and M. Ernzerhof, *Phys. Rev. Lett.*, 1996, **77**, 3865–3868.

47 J. P. Perdew, K. Burke and M. Ernzerhof, *Phys. Rev. Lett.*, 1997, **78**, 1396.

48 D. A. King and M. G. Wells, *Proc. R. Soc. London, Ser. A*, 1974, **339**, 245–269.

49 R. Bisson, M. Sacchi, T. T. Dang, B. Yoder, P. Maroni and R. D. Beck, *J. Phys. Chem. A*, 2007, **111**, 12679–12683.

50 A. C. Luntz, *J. Chem. Phys.*, 2000, **113**, 6901–6905.

51 R. R. Smith, D. R. Killelea, D. F. DelSesto and A. L. Utz, *Science*, 2004, **304**, 992–995.

52 M. G. Evans and M. Polanyi, *Trans. Faraday Soc.*, 1938, **34**, 0011–0023.

53 J. N. Bronsted, *Chem. Rev.*, 1928, **5**, 231–338.

This journal is © the Owner Societies 2013

Phys. Chem. Chem. Phys., 2013, **15**, 20526–20535 | **20535**